# Anharmonicity and phase stability of antiperovskite Li_{3}OCl

Min-Hua Chen, Alexandra Emly, and Anton Van der Ven

Phys. Rev. B **91**, 214306 — Published 18 June 2015

DOI: 10.1103/PhysRevB.91.214306

# Anharmonicity and Phase Stability of Anti-Perovskite $Li_3OCl$

Min-Hua Chen,[1,2] Alexandra Emly,[1] and Anton Van der Ven[2,*]

[1] *Department of Materials Science and Engineering, University of Michigan, Ann Arbor, Michigan 48109, USA*

[2] *Materials Department, University of California, Santa Barbara, California 93106, USA*

(Dated: June 2, 2015)

A lattice-dynamics study of the cubic $Li_3OCl$ anti-perovskite, a candidate solid electrolyte in lithium-ion batteries, reveals the presence of dynamical instabilities with respect to rotations of the $Li_6O$ octahedra. Calculated energy landscapes in the subspace of unstable octahedral rotational modes are very shallow with at most a 1 meV per formula unit reduction in energy upon breaking the cubic symmetry. While $Li_3OCl$ is not stable relative to decomposition into $Li_2O$ and LiCl at zero Kelvin, estimates of the vibrational free energy suggest that $Li_3OCl$ anti-perovskite should become entropically stabilized above approximately 480 K.

## I. INTRODUCTION

The recently discovered anti-perovskite $Li_3OCl$ compound is a promising solid electrolyte for Li-ion batteries, with ionic conductivities reported[1] to be almost as high as 2 mS $cm^{-1}$. $Li_3OCl$ has a perovskite crystal structure, but with the role of anions and cations reversed (Figure 1a): The positively charged Li ions form the corner sharing octahedra while the negatively charged O ions occupy the center of the Li-octahedra; the negatively charged Cl occupy the large cages at the center of the unit cell coordinated by 12 Li ions. Several first-principles studies of Li transport in the anti-perovskite crystal structure have predicted low migration barriers for Li-vacancy exchanges, with values on the order of 350 meV[2,3]. An even lower migration barrier of approximately 160 meV was predicted for an interstitial dumbbell mechanism[3]. The effect of alloying in $Li_3OCl_{1-x}Br_x$ on the migration barriers of vacancy mediated Li diffusion was also recently investigated from first-principles[4]. While Li vacancies and Li interstitials can appear at stoichiometric compositions through the creation of Frenkel defect pairs, the formation energy of such pairs is predicted to be too large[3] to achieve an appreciable concentration of diffusion mediating defects at room temperature. Off-stoichiometric compositions that are Li rich are likely more desirable to ensure an excess of Li ions that can migrate by means of the interstitial dumbell mechanism.

Devising strategies to synthesize off-stoichiometric compositions of $Li_3OCl$ by doping or alloying requires an understanding of the factors stabilizing $Li_3OCl$. First-principles studies predict that $Li_3OCl$ is metastable at zero Kelvin relative to decomposition into LiCl and $Li_2O$[2,3] (Figures 1b and 1c). The ability to synthesize $Li_3OCl$ experimentally[1], however, suggests that this compound is likely entropically stabilized at elevated temperatures, if not at room temperature, then at least at the higher synthesis temperatures of approximately $330 - 360°C$[1]. As $Li_3OCl$ does not exhibit significant configurational disorder and is an insulator, the most important degrees of freedom are vibrational excitations.

Perovskite structures have been widely studied. A perfectly cubic perovskite is rarely observed and most perovskites that exhibit cubic symmetry at high temperature undergo symmetry breaking transitions at low temperature. Symmetry breaking distortions can arise either as a result of distortions of the octahedra, or due to rotations of the octahedra[5]. The Glazer notation has been established to classify structures that can be derived from cubic perovskite through octahedral rotations[6]. Octahedral rotations around the three cubic axes are denoted with the notation $a^*b^*c^*$ where the letters $a$, $b$ and $c$ represent relative tilt angles around the cubic axes of the octahedra, and the $*$ can be $+$, $-$, or 0, depending on whether an in-phase, out-of-phase, or no tilt of neighboring octahedra has occurred[6]. In the case of the cubic $Pm\bar{3}m$ $Li_3OCl$ structure, which has no tilts, the tilt system is represented as $a^0a^0a^0$. Howard and Stokes have taken the 23 tilt systems proposed by Glazer[6] and using group-theory, simplified the list to 15 distinct tilt systems[7]. These group theoretic tools have proven invaluable in analyzing rotational instabilities in a wide range of perovskites[8–11].

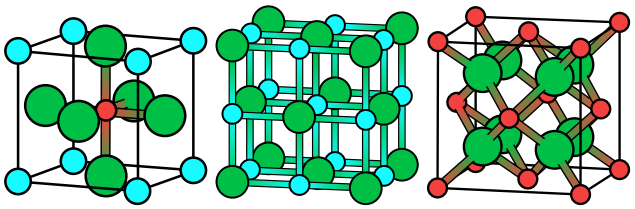

(a) (b) (c)

FIG. 1: (Color online) Crystal structures of (a) $Li_3OCl$, (b) LiCl, and (c) $Li_2O$. Lithium, oxygen, and chlorine atoms are represented by green, red, and blue circles, respectively.

In this work, we investigate the stability of $Li_3OCl$ using lattice dynamics. We find that $Li_3OCl$ is mechanically unstable with respect to octahedral rotations. We map out the energy landscape as a function of unstable modes and find that the minima correspond to several of the 14 rotational tilt systems[7]. The energy gained by octahedral rotations relative to the cubic crystal, how-

ever, is predicted to be very small, suggesting that the high-symmetry cubic form of $Li_3OCl$ should emerge even at low temperatures due to anharmonic vibrational excitations. Additionally, we find that vibrational entropy will likely stabilize the cubic $Pm\bar{3}m$ form of $Li_3OCl$ relative to decomposition into LiCl and $Li_2O$ above room temperature.

## II. METHODOLOGY

First-principles density functional calculations were performed using the Vienna Ab Initio Simulation Package (VASP)[12,13] within the generalized gradient approximation (GGA) as implemented by Perdew, Burke, and Ernzerhof[14]. Projector augmented wave[13,15] pseudopotentials with valence-electron configurations of $1s^1 2s^1 2p^1$ for Li, $2s^2 2p^4$ for O, and $3s^2 3p^5$ for Cl and an energy cutoff of 600 eV were used.

Force constants for $Li_3OCl$ were calculated using the frozen phonon approach. Isolated atomic displacements relative to their high symmetry positions in cubic antiperovskite were sampled in large supercells. The resulting forces on all the atoms in the supercell were then calculated with VASP. Force constants were determined using a least-squares fit between atomic perturbations and the calculated forces. The force constants were then used to construct the dynamical matrix[16–20]. Since $Li_3OCl$ is an ionic crystal, the effect of dipole-dipole interactions must also be accounted for in the dynamical matrix[21–23]. Born effective charges and dielectric tensors were calculated with density functional perturbation theory as implemented in VASP[24,25]. These were then used to calculate the non-analytic contribution to the dynamical matrix, which was evaluated within the same supercell as that for the atomic perturbations using the envelope function introduced by Wang et al[26]. A $6 \times 6 \times 6$ (1080 atoms) cubic supercell of the primitive cubic structures ($a = 3.907\mathring{A}$) was fully relaxed before applying various displacements of length $0.015\mathring{A}$ to each of the three asymmetric unit cell sites in the $Li_3OCl$ structure. A $3 \times 3 \times 3$ Gamma-centered $k$-point mesh was used in the VASP calculations performed on these supercells.

We also calculated vibrational free energies within the quasi-harmonic approximation for $Li_3OCl$, LiCl and $Li_2O$. Phonon dispersion curves and their corresponding densities of states were calculated as described above for a range of volumes. Smaller supercells were used for the quasi-harmonic calculations. For $Li_3OCl$, a $3 \times 3 \times 3$ supercell of the primitive cubic unit cell was used (containing 27 primitive cells and 135 atoms). For LiCl and $Li_2O$, supercells containing 32 unit cells (64 atoms) and 27 unit cells (81 atoms) were used. Atomic perturbations having lengths of 0.015, 0.15, and 0.03 $\mathring{A}$ for $Li_3OCl$, LiCl, and $Li_2O$, respectively were sampled to extract force constants. A second order polynomial fit of the free energy dependence on volume was used to obtain the Gibbs free energy as a function of temperature.

Irreducible representations of the $Pm\bar{3}m$ phase were obtained via the SMODES module of ISOTROPY (ISOTROPY Software Suite, iso.byu.edu). Accompanying each irreducible representation is one or more symmetrized collective displacement mode, each of which transforms the dynamical matrix into block diagonal form. The energy of the crystal was then calculated with VASP as a function of the amplitudes of the displacement modes. Energy calculations of collective displacements having $M_3^+$ and $R_4^+$ symmetries were performed in a supercell containing two primitive unit cells of $Li_3OCl$.

The FINDSYM module[27] of ISOTROPY was used to verify the space groups of the 15 structures resulting from octahedral tilts of the $Pm\bar{3}m$ structure. Structures were calculated using the same $2 \times 2 \times 2$ supercell of the 5 atom cubic primitive with a $9 \times 9 \times 9$ $\Gamma$-centered $k$-point mesh, thus ensuring that an identical k-point mesh was used for each structure. After a full relaxation of each structure, final energies were calculated using the tetrahedron method with Blöchl corrections[28].

## III. RESULTS

### A. Phonons

Figure 2 shows the calculated phonon dispersion curves for $Pm\bar{3}m$ $Li_3OCl$ as calculated using force constants fit to force-displacement relationships obtained from DFT-PBE calculations on a $6 \times 6 \times 6$ supercell of the cubic unit cell. We also show the dispersion curves using force constants extracted from a $3 \times 3 \times 3$ supercell. Because $Li_3OCl$ is an ionic crystal, contributions from Born effective charges were included in the calculation of the dispersion curves to account for macroscopic electric fields induced by long-range Coulombic interactions due to dipole moments that emerge from longitudinal optical phonons[16]. This leads to the LO-TO (longitudinal optical - transverse optical) splitting at the $\Gamma$ point[22,26]. Oxygen and chlorine occupy sites having cubic symmetry and therefore have isotropic Born effective charges with values of $-1.98|e|$ and $-1.30|e|$, respectively. The Li ions occupy sites with lower symmetry and have an anisotropic, diagonal Born effective charge tensor with a value of $0.99|e|$ in the direction of the O-Li-O bond and a value of $1.14|e|$ in the plane perpendicular to the O-Li-O bond. The dielectric tensor has diagonal elements of 15.13. The Born effective charges, particularly those of Li and O, are remarkably close to their formal charges, indicating the highly ionic nature of the material.

Figure 2 shows that the the cubic form of $Li_3OCl$ is dynamically unstable with respect to phonon modes at $R$ and $M$. The unstable modes, corresponding to imaginary eigenvalues of the dynamical matrix, are represented as negative frequencies in Figure 2. The instability at $R$ is three-fold degenerate, indicating that there are three symmetrically equivalent phonon modes that contribute to the decomposition of the cubic phase into a more ener-

getically favorable structure. Figure 2 also shows that a phonon mode at $M$ is slightly dynamically unstable when using force constants extracted from a $6 \times 6 \times 6$ supercell, and the same mode is predicted to be even more so when using force constants determined with a $3 \times 3 \times 3$ supercell.

The phonon density of states in Figure 2b show that the unstable modes account for a small fraction of the total phonon modes. The partial densities of states in Figure 2b indicate that the unstable modes involve only Li ions. The high frequency modes above approximately 5 THz are dominated by oxygen and Li. The Cl anions are about 5 times heavier than Li and reside in the large dodecahedrally coordinated cages characterized by long Cl-Li bonds. As a result, Cl accounts for most of the lower frequency stable modes.

The unstable modes at R indicate that the energy of the crystal can be lowered through octahedral tilts that generate the other 14 tilt systems. A systematic analysis can be accomplished by examining the irreducible representations of the point groups of the first Brillouin zone high-symmetry points[5] of cubic $Pm\bar{3}m$ $Li_3OCl$. In the anti-perovskite structure, the octahedral rotations result from positional displacements of the Li cations, while the O and Cl anions stay fixed. These rotations can be attributed to a six-dimensional reducible representation of $Pm\bar{3}m$, $M_3^+ \oplus R_4^+$, with $M_3^+$ and $R_4^+$ themselves being irreducible representations belonging to high-symmetry points $M$ and $R$ in the first Brillouin zone[7].

Distortions having $M_3^+$ symmetry can be characterized as rotations of all layers of octahedra around a single axis in a cooperative in-phase motion (Figure 3a), resulting in an $a^0a^0c^+$ tilt system and a $P4/mbm$ space group[7]. This tilt periodicity can be realized in a tetragonal supercell made up of two cubic primitive cells. Figure 3b shows the dependence of the energy of the crystal as the angle of rotation is incrementally increased. The energy well is highly anharmonic for small rotation angles varying by less than 0.2 meV over a two degree interval and exhibiting three local minima. The two minimia at nonzero rotation angle correspond to structures possessing $P4/mbm$ symmetry.

By doubling the $M_3^+$ unit cell in the $c$-axis direction, we effectively create two layers of octahedra that can be rotated in opposing directions, simulating an out-of-phase rotation between the two layers (Figure 3c). This distortion leads to the formation of a $a^0a^0c^-$ tilt system with a space group of $I4/mcm$. While the energy wells are slightly deeper than those of the $M_3^+$ rotation, the depth of the energy wells remain well above $-1$ meV per f.u. As is clear in Figures 3b and 3d, $M_3^+$ is indeed a stable mode, but both Figures 2c and 2a exhibit a relatively soft branch at $M$. This correlates with the ease at which the structure falls into the 2 energy minima when the $M_3^+$ distortion is applied.

At the R point, the $R_4^+$ representation is 3-fold degenerate, and each mode results in a rotation along a different pseudo-cubic axis (Figure 4). Defining the amplitudes of each of these rotational variants as order parameters $\xi_1, \xi_2, \xi_3$, we sampled distortions over a uniform grid in this three-dimensional space and calculated the energy landscape. A $\xi_1 = 0$ slice in the $\xi_1 - \xi_2 - \xi_3$ space is shown in Figure 5a. Similar to the $M_3^+$ rotations, the energy scales in the $\xi_2 - \xi_3$ space are extremely small, and the depth of the wells occur within 1 meV. Global energy minima are found along the [111] direction of the $\xi_1 - \xi_2 - \xi_3$ space. Taking two-dimensional slices along the [111], [110], and [100] directions in the $\xi_1 - \xi_2 - \xi_3$ space, we see in Figure 5b that while the lowest energy well occurs along [111], corresponding to an equal angle of rotation along each axis, it is less than half an meV lower than the energy wells along the [110] and [100] directions. We note that the minimum energy structures along the [111], [110], and [100] directions have space groups of $R\bar{3}c$, $Imma$, and $I4/mcm$, respectively. These space groups in turn correspond to the $a^-a^-a^-$, $a^0b^-b^-$, and $a^0a^0c^-$ tilt systems, which is consistent with conclusions drawn from previous group-theoretical analysis[5,29].

### B. Stability of $Pm\bar{3}m$ $Li_3OCl$ Relative to 14 Rotational Tilt Systems

Figure 6 shows the calculated energies of all 14 tilt systems relative to $Pm\bar{3}m$ $Li_3OCl$. The energies were calculated using the same $2 \times 2 \times 2$ supercell of the cubic primitive cell using an identical k-point mesh for each structure. All structures were allowed to relax fully. The space groups before and after relaxation were unchanged for each structure as verified using FINDSYM[27].

Of the 14 tilted structures, 10 have lower energy than the cubic $Pm\bar{3}m$. While Figure 6 shows that the introduction of octahedral tilts can lower the energy of the cubic anti-perovskite, it is important to note, however, that the energy differences between all 15 structures are within 1 meV per f.u. of each other. Despite minimizing $k$-point errors by using the same supercell for all calculations, the energy differences are small and still well within the numerical error range of first-principle calculations. The 15 different tilt systems in $Li_3OCl$ are therefore energetically indistinguishable, and it is impossible to unambiguously identify the most stable tilt system. It is also unlikely that the system will remain trapped in one of these lower symmetry distortions at all but the lowest temperatures.

### C. Stability of $Li_3OCl$ Relative to LiCl and $Li_2O$

$Li_3OCl$ at zero Kelvin is predicted to have a positive formation energy relative to a two phase mixture of $Li_2O$ and LiCl[3]. It is therefore not stable at zero Kelvin. It may, however, become entropically stabilized at elevated temperatures as a result of vibrational excitations. The unstable modes of cubic $Li_3OCl$ corresponding to the imaginary (negative) frequencies in Fig-

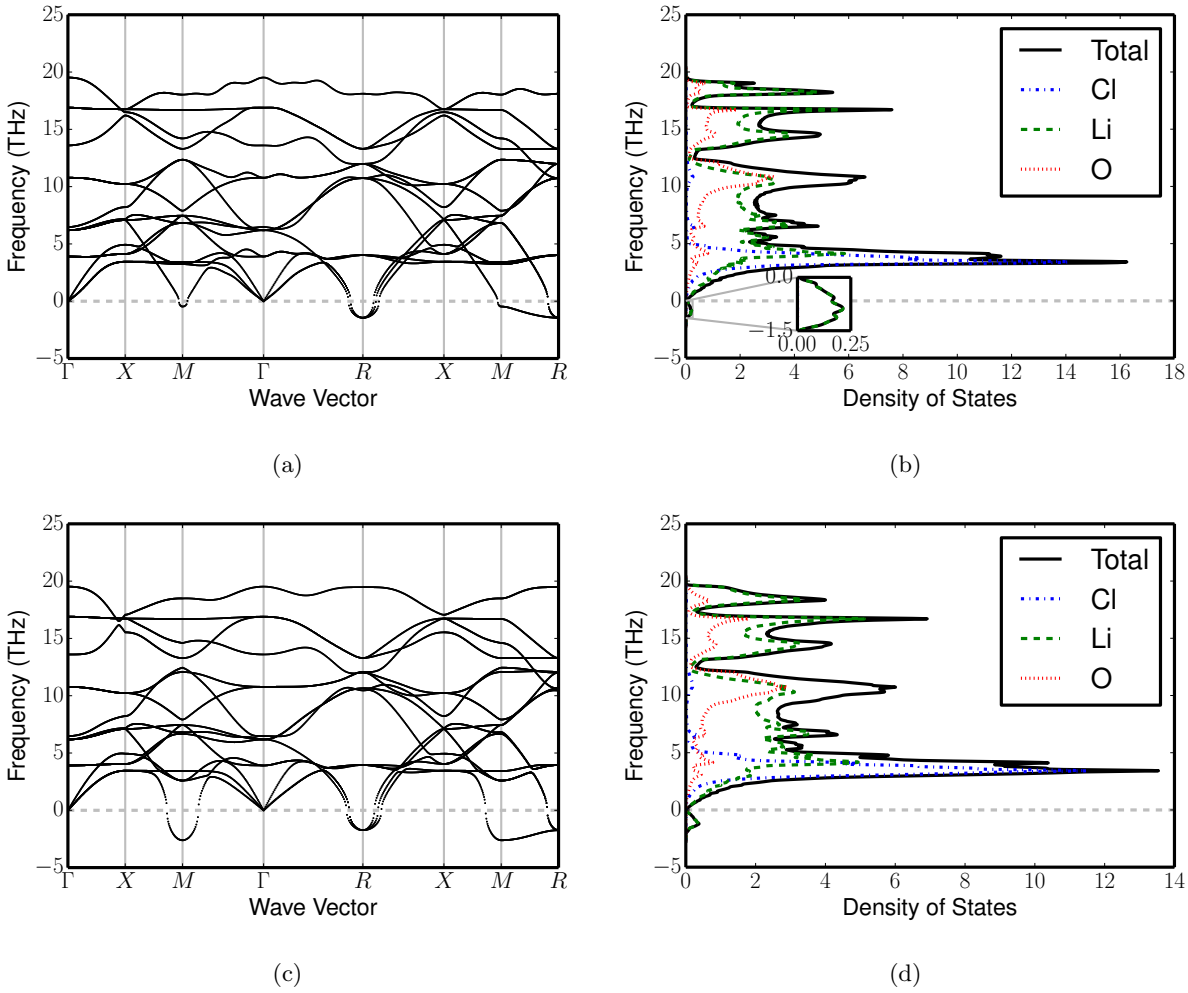


FIG. 2: (Color online) (a) Phonon dispersion curve and (b) density of states of $Pm\bar{3}m$ $Li_3OCl$ calculated using the finite displacement method with a lattice parameter of $3.907\mathring{A}$ and Born effective charge corrections in a $6 \times 6 \times 6$ supercell. (c) and (d) are the dispersion curve and density of states resulting from a $3 \times 3 \times 3$ supercell. There is a 3-fold degenerate instability at the Brillouin zone boundary $R$ point in both supercells, but the smaller supercell results in an instability at the $M$ point as well.

ures 2a and 2c pose challenges to calculating free energies at finite temperature using either the harmonic or quasi-harmonic approximation. The energy landscapes as a function of the amplitudes of the unstable phonon modes in Figures 3 and 5 reveal a substantial degree of anharmonicity with respect to $Li_6O$ octahedral rotational degrees of freedom. While instabilities and anharmonicity in materials have been extensively studied[30,31] and can be treated using first-principles parameterized anharmonic lattice-dynamical Hamiltonians together with Monte Carlo simulations[32–35], these approaches are highly involved. Here we estimate the free energy of $Li_3OCl$ within the quasi-harmonic approximation by integrating over only the stable phonon modes of cubic $Li_3OCl$ and argue that the neglect of unstable (anharmonic) modes should lead to an upper bound of the $Li_2O$ + LiCl to $Li_3OCl$ transition temperature.

To estimate the error incurred when calculating the free energy of a dynamically unstable high symmetry phase by integrating only over stable phonon modes, it is convenient to formally express the Born-Oppenheimer potential energy surface in terms of the amplitudes of phonon normal coordinates, $\xi_{\mathbf{k},b}$, where as usual, $\mathbf{k}$ refers to a wave vector and $b$ to a phonon branch. The potential energy surface can then be expressed as a polynomial expansion of the phonon normal coordinate amplitudes as, for example, described by Monserrat et al[36]. We can distinguish between two categories of phonon modes in such an expansion. For stable and stiff modes, the harmonic approximation should be suitable, and only terms up to second order need to be kept in the expansion. We will denote the amplitudes of these normal coordinates with $\xi^H_{\mathbf{k},b}$. For unstable or soft phonon modes, anharmonicity is important and polynomials of their amplitudes beyond

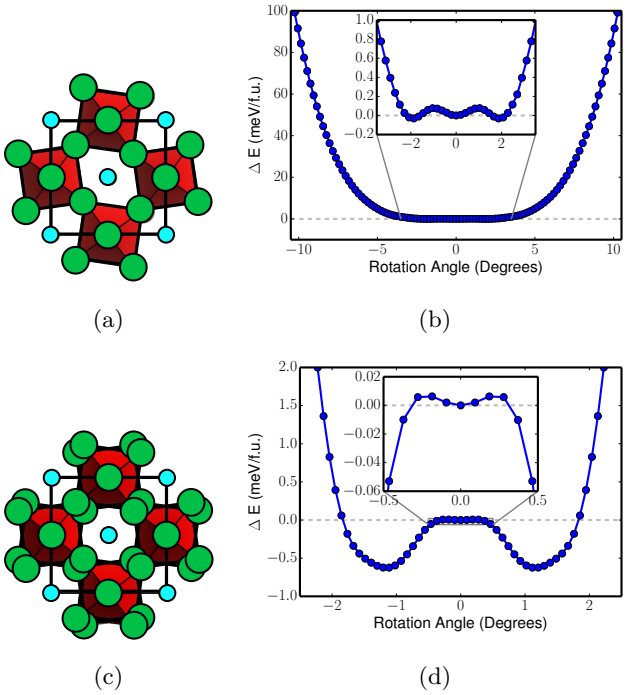


FIG. 3: (Color online) Energy variation with $Li_6O$ octahedral rotations. (a) In-phase octahedral rotations due to distortions with $M_3^+$ symmetry and (b) resulting energy variation. (c) Out-of-phase octahedral rotations and (d) resulting energy variation. Green, red, and blue circles represent Li, O, and Cl atoms, respectively. The zero reference energy is that of the undistorted $Pm\bar{3}m$ structure.

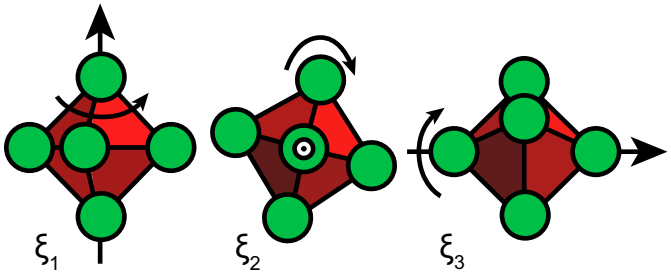


FIG. 4: (Color online) Octahedral tilts due to atomic displacements with the irreducible representation symmetry $R_4^+$. The three-fold degeneracy of $R_4^+$ leads to three variants of this distortion, where each variation is an octahedral rotation about a different axes.

the second order are needed to reproduce the full potential energy surface. We denote the amplitudes of these phonon modes with $\xi^A_{\mathbf{k}',b'}$. The potential energy surface can then formally be written as

$$V\left(\{\xi^H_{\mathbf{k},b}\},\{\xi^A_{\mathbf{k}',b'}\}\right) = \sum_{\mathbf{k},b}\frac{1}{2}\omega^2_{\mathbf{k},b}(\xi^H_{\mathbf{k},b})^2$$

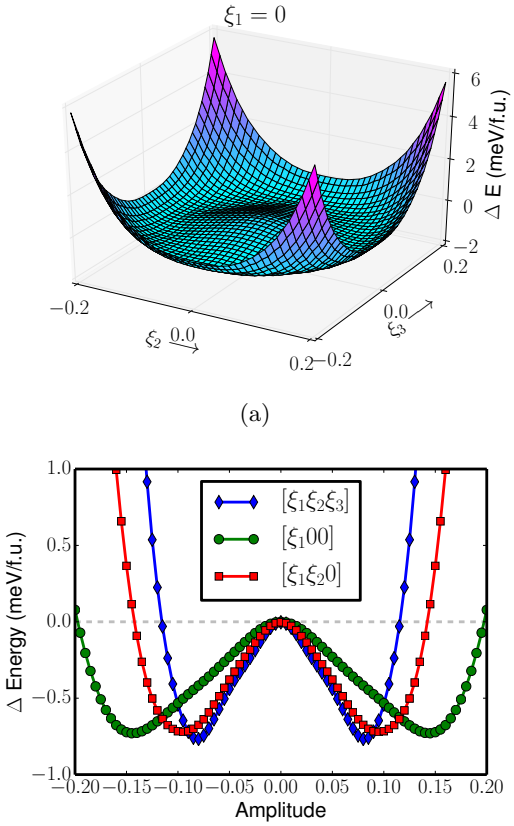


FIG. 5: (Color online) Energy variations due to distortions with $R_4^+$ symmetry with $Pm\bar{3}m$ as the energy reference. (a) The energy landscape of an $\xi_1 = 0$ slice of the 3-D $\xi_x$ space. The landscape is very flat, with the energy scale around the wells being on the order of 1 meV/f.u. (b) Amplitude dependent energies in the [111], [110], and [100] directions of the $\xi_x$ space leading to the formation of $R\bar{3}c$, $Imma$, and $I4/mcm$ structures.

$$+ V^A\left(\{\xi^A_{\mathbf{k}',b'}\}\right). \qquad (1)$$

where the $\xi^A_{\mathbf{k}',b'}$ appearing in the anharmonic potential $V^A(\xi^A_{\mathbf{k}',b'})$ may even be coupled to each other. With this partitioning, it is next convenient to split the full vibrational Hamiltonian, including the kinetic energy, into a sum of a harmonic part $H^H$ and an anharmonic part $H^A$ where

$$H^H = \sum_{\mathbf{k},b}\left(\frac{(\dot{\xi}^H_{\mathbf{k},b})^2}{2} + \frac{1}{2}\omega^2_{\mathbf{k}}(\xi^H_{\mathbf{k},b})^2\right) \qquad (2)$$

$$H^A = \sum_{\mathbf{k}',b'}\frac{(\dot{\xi}^A_{\mathbf{k}',b'})^2}{2} + V^A\left(\{\xi^A_{\mathbf{k}',b'}\}\right). \qquad (3)$$

Since $H^H$ and $H^A$ are decoupled from each other, they

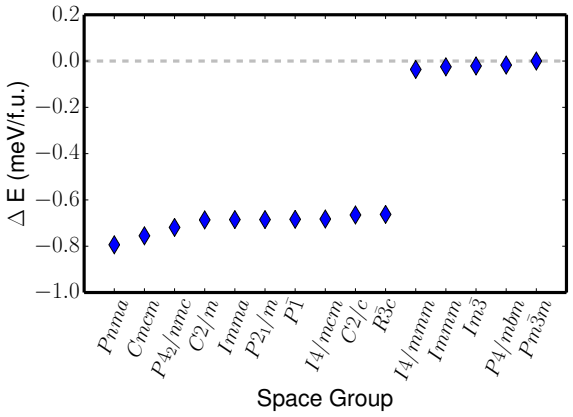


FIG. 6: (Color online) Energies of $Li_3OCl$ in the 15 tilt systems. The $Pm\bar{3}m$ structure was used as the reference. All distortions were calculated in a $2 \times 2 \times 2$ supercell of the primitive cell to minimize $k$-point errors. The energies are within 0.8 meV of the perfect cubic structure.

can be solved separately. The harmonic Hamiltonian will have energy levels $E_\nu^H = \sum_{\mathbf{k},b} \hbar\omega_{\mathbf{k},b} \left(n_{\mathbf{k},b} + 1/2\right)$ where the $n_{\mathbf{k},b}$ are integer quantum numbers. Formal solutions to the anharmonic Hamiltonian will generate a spectrum of energy levels $E_0^A, E_1^A, \ldots, E_{\nu'}^A, \ldots$ , where $E_0^A$ corresponds to the ground state energy of the anharmonic Hamiltonian. The energy of any particular vibrational microstate $\eta$ of the full crystal is then

$$E_\eta = E^o_{\text{cubic}} + \sum_{\mathbf{k},b} \hbar\omega_{\mathbf{k},b} \left(n_{\mathbf{k},b} + 1/2\right) + E_0^A + \Delta E_{\nu'}^A \quad (4)$$

where $E^o_{\text{cubic}}$ is the fully relaxed energy of cubic $Li_3OCl$ and $\Delta E_{\nu'}^A = E_{\nu'}^A - E_0^A$ (which is always $\geq 0$).

Substitution of Eq. 4 into the partition function $Z = \sum_\eta \exp(-\beta E_\eta)$ and using $F = -(1/\beta)\ln Z$ yields a free energy $F$ that can be written as a sum of a harmonic vibrational free energy $F^H$ and an anharmonic free energy contribution $F^A$. An explicit expression for $F^H$ can only be derived once a criterium is established to distinguish between the phonon modes appearing in the harmonic Hamiltonian and those appearing in the anharmonic Hamiltonian. Here we assume that all stable phonon modes fall in the first category while all unstable phonon modes fall in the second category. The free energies can then be written as

$$F^H = E^\circ_{\text{cubic}} + E^H_{\text{zp}} + \frac{1}{\beta}\int_0^\infty g(\omega)\ln\left(1 - \exp\left(-\beta\hbar\omega\right)\right) d\omega \quad (5)$$

and

$$F^A = E_0^A - \frac{1}{\beta}\ln\left(\sum_{\nu'} \exp\left(-\beta\Delta E_{\nu'}^A\right)\right). \quad (6)$$

$E^H_{\text{zp}}$ appearing in Eq. 5 refers to the zero point energy of the harmonic Hamiltonian and is given by

$$E^H_{\text{zp}} = \int_0^\infty \frac{1}{2} g(\omega)\hbar\omega d\omega \quad (7)$$

where $g(\omega)$ is the density of states.

The harmonic free energy $F^H$ can be calculated numerically given the vibrational density of states $g(\omega)$ (Figure 2b and 2d) by integrating over solely the stable phonon frequencies in the Brillouin zone. The anharmonic contribution $F^A$ due to the presence of soft, unstable modes, however, is not as accessible. It consists of a temperature independent term $E_0^A$ which could be positive or negative and a temperature dependent term, $-k_BT\ln\left(\sum_{\nu'}\exp\left(-\beta\Delta E_{\nu'}^A\right)\right)$, which is always negative. The second term of $F^A$, therefore, lowers the total free energy and gives it a more negative slope as a function of temperature compared to that of $F^H$. If $E_0^A$ is zero or negative, then the true free energy $F$ will be less than $F^H$ at all temperatures. If $E_0^A$ is positive, however, its inclusion in the estimate of $F$ will result in a rigid upward shift of the free energy curve as a function of temperature relative to $F^H$.

The order of magnitude of $E_0^A$ can be estimated by comparing the zero Kelvin component of the free energy of cubic $Li_3OCl$, $E^o_{\text{cubic}} + E^H_{\text{zp}} + E_0^A$, to the zero Kelvin free energy of a dynamically stable tilted variant of cubic $Li_3OCl$. The lower symmetry $I4/mcm$ form of $Li_3OCl$, for example, is dynamically stable. Within the harmonic approximation, its free energy at zero Kelvin is equal to the fully relaxed energy $E_{I4/mcm}$ plus its zero point energy $E^{\text{zp}}_{I4/mcm}$. The two free energies at zero Kelvin should be very similar, if not equal, i.e.

$$E^o_{\text{cubic}} + E^H_{\text{zp}} + E_0^A = E_{I4/mcm} + E^{\text{zp}}_{I4/mcm} \quad (8)$$

provided that the harmonic approximation at zero Kelvin is valid for the $I4/mcm$ form of $Li_3OCl$ and that the decomposition in harmonic and anharmonic free energies is sufficiently accurate for the cubic form of $Li_3OCl$. Based on Eq. 8 and a calculation of the phonon density of states for the $I4/mcm$ form of $Li_3OCl$, we estimate a value for $E_0^A$ of approximately 5 meV per $Li_3OCl$ formula unit. Although $E_0^A$ is positive, its magnitude still suggests that $E_0^A$ has a negligible contribution to the total free energy $F$ of cubic $Li_3OCl$ and that $F^H$ can therefore serve as an upper bound to the true free energy of $Li_3OCl$. The transition temperature for the LiCl plus $Li_2O$ reaction to $Li_3OCl$ using $F^H$ instead of $F$ should therefore serve as an upper bound to the true transition temperature.

We estimate the temperature at which $Li_3OCl$ is stabilized relative to LiCl and $Li_2O$ by first conducting quasi-harmonic calculations for all three phases. The quasi-harmonic approximation, unlike the purely harmonic model, accounts for thermal expansion by constructing volume dependent free energies. These volume and temperature dependent free energy curves, $F(T,V) = E(V) + F^H(T,V)$, consist of the energy of a

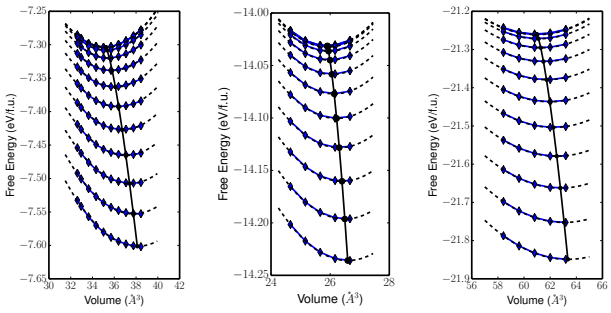


(a) (b) (c)

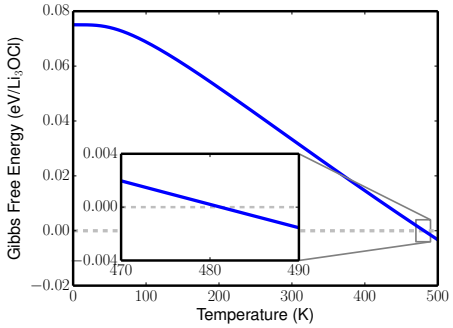


(d)

FIG. 7: (Color online) Quasi-harmonic curves for (a) LiCl, (b) $Li_2O$, and (c) $Li_3OCl$ and (d) free energy curve for $Li_3OCl$. Volume-free energy curves are at increments of 50 K between 0 - 550 K. $Li_3OCl$ is entropically stabilized at 480 K, which is an upper-bound approximation.

static lattice at a particular volume, $V$, and the harmonic vibrational free energy at the same volume. Minimizing $F(T,V)$ with respect to $V$ results in the Gibbs free energy at zero pressure. Harmonic phonons were calculated at volumes both larger and smaller than the equilibrium volume for LiCl, $Li_2O$, and $Li_3OCl$. Both LiCl and $Li_2O$ were predicted to be dynamically stable, having only real phonon frequencies. The phonon density of states corresponding to the real vibrational frequencies were used to obtain $F^H(T,V)$ for each of the three phases, which are shown in Figures 7a, 7b, and 7c.

In determining the force constants at different volumes for the quasi-harmonic free energies of $Li_3OCl$, we used a $3\times3\times3$ supercell (containing 135 atoms) as opposed to the substantially larger $6\times6\times6$ supercell (containing 1080 atoms) used to extract force constants for our initial phonon analysis. The dispersion curves resulting from the force constants extracted from the $3\times3\times3$ supercell exhibit softer modes both at $R$ and $M$ (Figure 2c) than those based on a $6\times6\times6$ supercell. This is likey due to the sampling of anharmonic modes and the ease with which a slight 1° rotation of the $Li_6O$ octahedra nudges the system into a lower energy state. Note in Figure 2d that the soft mode contribution to the total density of states is very small. Using the Gibbs free energies for each of the three compounds, we can calculate a formation free energy for $Li_3OCl$, $\Delta G_{Li_3OCl} = G_{Li_3OCl} - G_{LiCl} - G_{Li_2O}$. Figure 7d, shows that an upper bound temperature at which $Li_3OCl$ is stabilized is approximately 480 K. Errors of $+/-1$ meV per formula unit of $Li_3OCl$ bring the transition temperature within a range of 475 - 487 K, while errors of $+/-5$ meV per formula unit of $Li_3OCl$ result in bounds of 450 - 510 K.

## IV. DISCUSSION

$Li_3OCl$ shows promise as a solid electrolyte for Li-ion batteries[1]. It is, however, predicted to have a positive formation energy relative to a two-phase mixture of LiCl and $Li_2O$[2,3]. Furthermore, to ensure a high concentration of diffusion mediating defects, the compound must be synthesized with a composition that deviates from perfect stoichiometry as the energy to form Frenkel pairs in the stoichiometric compound is too high to generate a sufficient number of Li interstitials and vacancies at room temperature[3]. A deeper understanding of the factors responsible for the observed stability of $Li_3OCl$ is therefore desirable.

Our analysis of the phonon modes of $Li_3OCl$ shows that its cubic form is dynamically unstable with respect to $Li_6O$ octahedral rotations. The instability occurs at the $R$ wave vector points and leads to the spontaneous decomposition of $Pm\bar{3}m$ $Li_3OCl$ into lower energy tilt systems, which has been observed in other perovskite materials[10,37]. $Li_3OCl$ is highly anharmonic with respect to rotational degrees of freedom of the $Li_6O$ octahedra. The energy landscape as a function of unstable phonon modes of cubic $Li_3OCl$ is very shallow (Figure 5a) with the energy differences between cubic and lower symmetry tilt systems being too small to establish which distortion is more stable (Figure 6). It is therefore unlikely that any of the lower symmetry tilt variants of $Li_3OCl$ will be stable at any but the lowest temperatures, becoming cubic when sufficient thermal energy is available to overcome the smal energy barriers separating the various low symmetry variants.

The ionic radius of Cl relative to Li and O is consistent with the Goldschmidt rule[38] for cubic perovskite stability with respect to rotational instabilities of the $Li_6O$ octahedra. General guidelines indicate that a cubic structure is preferred for a tolerance factor, defined for an $ABX_3$ perovskite as

$$t = \frac{(R_A+R_X)}{\sqrt{2}(R_B+R_X)}, \tag{9}$$

between $0.9-1$. The tolerance factor for $Li_3OCl$ is 0.84, based on ionic radii tabulated by Shannon[39]. Substituting Cl with a larger anion should make the cubic perovskite dynamically stable with respect to $Li_6O$ octahedral rotations. Br, for example, which has been alloyed on the Cl sublattice of $Li_3OCl$ to optimize Li conductivity[1,3,4], results in a slightly higher tolerance

factor of 0.89 for $Li_3OBr$. This suggests that $Li_3OBr$ is unlikely to exhibit rotational instabilities.

While our analysis of phase stability due to vibrational excitations does not rigorously account for anharmonicity, it does give a strong indication that $Li_3OCl$ should be entropically stabilized at high temperature. Nevertheless the precise temperature above which $Li_3OCl$ should become thermodynamically stable relative to LiCl+$Li_2O$ is uncertain as our quasi-harmonic model and subsequent analysis only provide an upper bound estimate. Our results, however, indicate that $Li_3OCl$ is very likely stable at typical synthesis temperatures of 330-360°C[1]. Because our free energy calculations relied on the density of states corresponding to stable phonon modes, we were unable to account for the anharmonic contributions to the free energy. The contribution to the total density of states by the imaginary frequencies, however, is relatively small when extracting force constants from frozen phonon calculations using the 1080 or 135 atom supercells of $Li_3OCl$. This suggests that the inclusion of anharmonic excitations is unlikely to have a strong effect on the predicted temperature above which $Li_3OCl$ becomes stable relative to LiCl and $Li_2O$.

The phonon analysis of $Li_3OCl$ provides insight about the factors responsible for the high temperature stability of $Li_3OCl$. As shown in the partial densities of states of Figures 2b and 2d, the majority of the low frequency modes can be attributed to Cl anions and Li cations, while the majority of high frequency modes involve both Li and O. Cl in $Li_3OCl$ resides in a large cage and is 12 fold coordinated by Li, which is substantially higher than its 6-fold coordination in LiCl. The Li-Cl bond lengths in $Li_3OCl$ are 2.76$\mathring{A}$, which are longer than the 2.58$\mathring{A}$ Li-Cl bonds in LiCl. Longer bonds tend to be softer, resulting in an increase in vibrational entropy[20]. Hence Cl will gain in vibrational entropy when going from its octahedrally coordinated sites in LiCl to the more open 12-fold coordinated sites in $Li_3OCl$. Additional vibrational entropy arises from the easy $Li_6O$ octahedral rotations, a degree of freedom that is absent in the more compact LiCl and $Li_2O$ phases.

At practical temperatures for Li-ion battery applications, the $Li_6O$ rotational tilts will be energetically accessible due to thermal excitations. While these tilts will have consequences for ion transport, it is unclear whether the rotational instabilities will facilitate or hinder Li diffusion. Transition state theory assumes that the initial and final states are dynamically stable, which is not the case here for cubic $Li_3OCl$. Understanding the role of octahedral rotations on Li diffusion in $Li_3OCl$, either by a vacancy or interstitial dumbbell mechanism, will require analysis of molecular dynamics simulations at temperatures where the cubic form of $Li_3OCl$ is stabilized by anharmonic vibrational excitations.

## V. CONCLUSION

Through a harmonic phonon model we have shown that the cubic $Pm\bar{3}m$ $Li_3OCl$ structure, which has been known to be metastable[2,3], is mechanically unstable. Aided by group-theoretical analysis, we have identified that a combination of the three degenerate unstable modes with $R_4^+$ symmetry can result in lower-energy tilt systems. Furthermore, we have explored the energetics of $M_3^+$, the other irreducible representation known for inducing octahedral rotations. Calculations of the 15 tilt systems showed that while structures involving octahedral tilts have lower energy than cubic $Pm\bar{3}m$, energy differences are too small to identify a single system as most stable. We have also found that $Li_3OCl$ is indeed stabilized by vibrational entropy at temperatures lower than 480 K.

## ACKNOWLEDGMENTS

We thank Dr. John C. Thomas for his contributions to the phonon code used in this work and for helpful discussions. This material is based upon work supported by the National Science Foundation, Grant No. DMR-1410242. Resources of the National Energy Research Scientific Computing Center, which is supported by the Office of Science of the U.S. Department of Energy under Contract No. DE-AC02-05CH11231 are gratefully acknowledged, in addition to support from the Center for Scientific Computing at the CNSI and MRL: an NSF MRSEC (DMR-1121053) and NSF CNS-0960316. Crystal structure images were generated using VESTA[40].

* avdv@engineering.ucsb.edu

[1] Y. Zhao and L. L. Daemen, Journal of the American Chemical Society **134**, 15042 (2012), pMID: 22849550, http://dx.doi.org/10.1021/ja305709z.
[2] Y. Zhang, Y. Zhao, and C. Chen, Phys. Rev. B **87**, 134303 (2013).
[3] A. Emly, E. Kioupakis, and A. Van der Ven, Chemistry of Materials **25**, 4663 (2013), http://dx.doi.org/10.1021/cm4016222.
[4] Z. Deng, B. Radhakrishnan, and S. P. Ong, Chemistry of Materials **27**, 3749 (2015), http://dx.doi.org/10.1021/acs.chemmater.5b00988.
[5] M. A. Carpenter and C. J. Howard, Acta Crystallographica Section B **65**, 134 (2009).
[6] A. M. Glazer, Acta Crystallographica Section B **28**, 3384 (1972).
[7] C. J. Howard and H. T. Stokes, Acta Crystallographica Section B **54**, 782 (1998).
[8] N. A. Benedek and C. J. Fennie, The Journal of Physical Chemistry C **117**, 13339 (2013), http://dx.doi.org/10.1021/jp402046t.

[9] M. A. Islam, J. M. Rondinelli, and J. E. Spanier, Journal of Physics: Condensed Matter **25**, 175902 (2013).
[10] K. Z. Rushchanskii, N. A. Spaldin, and M. Ležaić, Phys. Rev. B **85**, 104109 (2012).
[11] G. Gou, I. Grinberg, A. M. Rappe, and J. M. Rondinelli, Phys. Rev. B **84**, 144101 (2011).
[12] G. Kresse and D. Joubert, Phys. Rev. B **59**, 1758 (1999).
[13] G. Kresse and J. Furthmüller, Phys. Rev. B **54**, 11169 (1996).
[14] J. P. Perdew, K. Burke, and M. Ernzerhof, Phys. Rev. Lett. **77**, 3865 (1996).
[15] P. E. Blöchl, Phys. Rev. B **50**, 17953 (1994).
[16] M. Born and K. Huang, *Dynamical theory of crystal lattices*, International series of monographs on physics (Clarendon Press, 1954).
[17] S. Wei and M. Y. Chou, Phys. Rev. Lett. **69**, 2799 (1992).
[18] K. Parlinski, Z.-. Q. Li, and Y. Kawazoe, Phys. Rev. Lett. **78**, 4063 (1997).
[19] X. Gonze and C. Lee, Phys. Rev. B **55**, 10355 (1997).
[20] A. van de Walle and G. Ceder, Rev. Mod. Phys. **74**, 11 (2002).
[21] R. Lyddane, R. Sachs, and E. Teller, Phys. Rev. **59**, 673 (1941).
[22] W. Cochran and R. Cowley, Journal of Physics and Chemistry of Solids **23**, 447 (1962).
[23] S. Baroni, S. de Gironcoli, A. Dal Corso, and P. Giannozzi, Rev. Mod. Phys. **73**, 515 (2001).
[24] P. Giannozzi, S. de Gironcoli, P. Pavone, and S. Baroni, Phys. Rev. B **43**, 7231 (1991).
[25] M. Gajdoš, K. Hummer, G. Kresse, J. Furthmüller, and F. Bechstedt, Phys. Rev. B **73**, 045112 (2006).
[26] Y. Wang, S. Shang, Z.-K. Liu, and L.-Q. Chen, Phys. Rev. B **85**, 224303 (2012).
[27] H. T. Stokes and D. M. Hatch, Journal of Applied Crystallography **38**, 237 (2005).
[28] P. E. Blöchl, O. Jepsen, and O. K. Andersen, Phys. Rev. B **49**, 16223 (1994).
[29] P. V. Balachandran and J. M. Rondinelli, Phys. Rev. B **88**, 054101 (2013).
[30] K. Persson, M. Ekman, and V. Ozoliņš, Phys. Rev. B **61**, 11221 (2000).
[31] G. Grimvall, B. Magyari-Köpe, V. Ozoliņš, and K. A. Persson, Rev. Mod. Phys. **84**, 945 (2012).
[32] W. Zhong, D. Vanderbilt, and K. M. Rabe, Phys. Rev. Lett. **73**, 1861 (1994).
[33] W. Zhong, D. Vanderbilt, and K. M. Rabe, Phys. Rev. B **52**, 6301 (1995).
[34] J. Bhattacharya and A. Van der Ven, Acta Materialia **56**, 4226 (2008).
[35] J. C. Thomas and A. Van der Ven, Phys. Rev. B **88**, 214111 (2013).
[36] B. Monserrat, N. D. Drummond, and R. J. Needs, Phys. Rev. B **87**, 144302 (2013).
[37] H. Sim and B. G. Kim, Phys. Rev. B **89**, 201107 (2014).
[38] V. Goldschmidt, Naturwissenschaften **14**, 477 (1926).
[39] R. D. Shannon, Acta Crystallographica Section A **32**, 751 (1976).
[40] K. Momma and F. Izumi, Journal of Applied Crystallography **41**, 653 (2008).